Engineered Science
DOI: https://dx.doi.org/10.30919/es901

Numerical Study of Cough Droplets Evaporation and Dispersion in an Indoor Environment Using the Multi-component Eulerian-Lagrangian Approach

Chartchay Chumchan,[1] Bunyong Rungroungdouyboon[2] and Phadungsak Rattanadecho[3,*]

Abstract

The purpose of this study was to identify the relationship between human performance and heat map entropy in a system state judgment task through the visual interface screen. A prototype of an EID-based accident response support system was used as the visual interface screen for the experiment. Sixteen subjects performed an experiment in which the system state was judged based on the problems presented by the experimenter through the visual interface screen. The experimental results confirmed that the heat map entropy increased as the time to judge the system state increased. In addition, it was confirmed that the heat map entropy of cases that did not correctly judge the system state was significantly greater than that of cases that correctly judged the system state. It was found that a close relationship existed between the performance of judging the system state from the visual interface screen and heat map entropy. This means that it can predict human performance based on heat map entropy. Therefore, heat map entropy can be used to evaluate the suitability of the visual interface design.

Keywords: SARS-CoV-2-laden cough droplets; Cough droplets; Evaporation; Droplet nuclei; Multi-component Eulerian-Lagrangian model.
Received: 06 December 2022; Revised: 14 April 2023; Accepted: 25 May 2023.
Article type: Research article.

1. Introduction

It is now known for certain that the SARS-CoV-2 virus that is contained within the droplets of COVID-19 can be transmitted through the aerosols produced when affected people breathe or sneeze.[1] Large droplets are produced from saliva during activities such as sneezing and wheezing, and microscopic droplets are created by coating the mucous membranes of the airways and the vocal cords. The larger particles can sometimes be seen with the unaided eye, but the smaller ones are usually obscured. Depending on the ventilation in the region, the droplets may transport contagious agents such as pathogens or viral groups into the air, which may lead to the spread of infectious illnesses. In most cases, the droplet containing pathogens is generated when a person who is affected coughs or sneezes, which is the process that causes sneezing fog with numerous droplets. The force of gravity caused enormous droplets to fall to the ground in a relatively brief amount of time. The residual particles are known as droplets nuclei or aerosols and have the ability to transfer pathogens over longer distances. Small droplets have the ability to remain airborne for extended periods of time, but they have a tendency to dissipate quickly in dry air.[2,3] Additional particle nuclei that are kept in the air by a combination of buoyancy and temperature forces.[4] Suspend the droplet after it has been adsorbed on the small solid particles in order to progressively generate bioaerosol particles in the droplet nucleus. As far back as the 1940s, Duguid (1946) studied the size of droplets from speaking, coughing and sneezing through microscopic measurements and found that the droplet diameter ranged from 1μm to 2,000 μm and that 95% of the droplets are smaller than 100 μm.[5] In a study by

[1] *Department of Power Engineering Technology, College of Industrial Technology, King Mongkut's University of Technology North Bangkok, Bangkok, 10800, Thailand.*
[2] *Center of Excellence in Creative Engineering Design and Development (CED2), Department of Mechanical Engineering, Faculty of Engineering, Thammasat University (Rangsit Campus), Pathum Thani 12121, Thailand*
[3] *Center of Excellence in Electromagnetic Energy Utilization in Engineering (C.E.E.E.), Department of Mechanical Engineering, Faculty of Engineering, Thammasat University (Rangsit Campus), Pathum Thani, 12120, Thailand.*
**Email:* ratphadu@engr.tu.ac.th (P. Rattanadecho)

Kwak *et al.*, saliva evaporates slowly compared to water droplets due to the attraction of ions/proteins in the saliva.[6] Additionally, droplets on the ground may rise into the air again because of evaporation.[7] For droplets ranging in diameter from 1 to 1,000 µm, wells[8] and Xie *et al.*[9] compared the time for complete evaporation of isolated droplets to their settling time and reported that drops with diameter d > 100 µm settle in liquid form to the ground in less than one second. The computational fluid dynamics (CFD) analysis should be achieved in a satisfactory agreement, which must predict the evaporation and dispersion of the droplets that convert into the solid droplet nuclei. Since the outbreak of COVID-19, most scientists have focused their attention on predicting the respiratory droplets produced by people infected with the virus to different areas and environments using experiments and numerical study. The relevant literature contains experimental studies and numerical studies using Euler-Euler or Euler-Lagrange based models.[1,7,9-19] Several studies have neglected the mechanism of evaporation became to nuclei (aerosol) of the cough droplets, which may limit the validity of droplet nuclei trajectory predictions. However, respiratory droplets are composed of water and a small number of non-volatile compounds that can represent viral load. In the literature review, only a few papers propose the numerical model to investigate the water in the droplet evaporates of exhalation and cough in the various ambient conditions and ultimately leaves the non-volatile components into the solid droplet nuclei as follows. Chen and Zhao employ a numerical model to investigate the dispersion characteristics of human exhaled droplets in ventilation rooms.[20] Yang *et al.* investigated the impact of initial droplet size to simulate the dispersion process of the droplets with an initial diameter of 10 µm and 100 µm, and gaseous contaminant in a unidirectional ventilated protective isolation room and studied the droplets dispersion and cross-transmission with different sizes.[21] Li *et al.* proposes the modeling of evaporation of cough droplets in inhomogeneous humidity fields using the multi-component Eulerian-Lagrangian approach to investigate the cough droplet transport and size change dynamics in a static ambient air condition.[22] The multi-component Eulerian-Lagrangian model was employed to realize the mechanistic modelling of droplet evaporation process of the thermal effect of the human body on the evaporation of the cough droplets in an enclosed space.[23] Calmet *et al.* used a highly resolved mesh of large eddy simulation to capture the multiphase turbulent buoyant cloud with suspended droplets produced by a cough. The cough droplets' dispersion was subjected to thermal gradients and evaporation and allowed to disperse between two humans standing 2 m apart.[24]

In this study, droplet evaporation and dispersion are provided by using numerical modeling to understand the basic aerosol science of SARS-CoV-2-laden droplets spread through the air of indoor environment as quasi-quiescent air. Numerical modeling can be extended to provide high resolution on the transport of infected aerosols and prediction of their accumulation from the human respiratory system. To estimate the RNA load of SARS-CoV-2 in a room or enclosed space. To further understand viral infection, replication, and disease pathogenesis in the near future and to better prepare for the post-epidemic phase and have a high chance of resuscitation. Although, an isolation room, the pressurization specification can be achieved by exhausting at least 15% more air than the supply air with 6-12 ACH[25,26] but for an indoor environment, it is not ensured for guarantees a reduction of viral transmission from cough droplets. Therefore, to study the mitigation strategies for reducing viral transmission in the ventilation design for various indoor environments, the generation of solid droplet nuclei from coughing, sneezing, and talking has inspired the use of numerical simulation, which investigates the droplet-laden cough jet with the reality of the spread of pathogens. Consequently, this research objective proposed the numerical study with the multi-component Eulerian-Lagrangian approach to study droplet evaporation and dispersion in quiescent air. The size reduction until became droplet nuclei and trajectory of the cough droplets were predicted to study the influent temperatures with specific relative humidity.

2. Governing equations

In the governing equations, the RNG k-ε model is coupled with a Discrete Phase Model (DPM), energy equation, and species transport equation. The RNG k–ε model can be predicted more swirls and more complex trajectories.[4,21,22,25,27] The multi-component Eulerian-Lagrangian model was applied to realize the mechanism of droplet evaporation process. The flow has two phases: the carrier phase (air) and the discrete phase (droplets and droplet nuclei). The carrier phase is modeled by Eulerian model whereas the discrete phase is modeled by Lagrangian model. Expression for continuity, momentum, energy, species, turbulent model, DPM model are as follows:[28]

$$\frac{\partial \rho}{\partial t} + \nabla . (\rho \vec{v}) = S_m \quad (1)$$

where ρ and $\vec{v}$ are gas density and velocity, and S_m is mass source term.

$$\frac{\partial}{\partial t}(\rho \vec{v}) + \nabla . (\rho \vec{v} \vec{v}) = -\nabla p + \nabla . (\overline{\tau}) + \rho \vec{g} + U_p S_m + \vec{F}_{gp} \quad (2)$$

where p is the static pressure, $\overline{\tau}$is the stress tensor (described below), $\rho \vec{g}$is the gravitational body force. $\vec{F}_{gp}$is sum of the forces exerted by particles on the gas phase.

$$\overline{\tau} = \mu \left[(\nabla \vec{v} + \nabla \vec{v}^T) - \frac{2}{3} \nabla . \vec{v} I \right] \quad (3)$$

where μ is the molecular viscosity, I is the unit tensor, and the second term on the right hand side is the effect of volume dilation.

$$\frac{\partial}{\partial t}\left(\rho\left(e + \frac{v^2}{2}\right)\right) + \nabla .\left(\rho v\left(h + \frac{v^2}{2}\right)\right) = \nabla .\left(k_{eff} \nabla T - \sum_j h_j \vec{J}_j + \overline{\tau}_{eff} . \vec{v}\right) + S_h \quad (4)$$

where k_{eff} is the effective conductivity, $\vec{J}_j$and is the diffusion flux of species, j. The first three terms on the right-hand side

of Eq.4 represent energy transfer due to conduction, species diffusion, and viscous dissipation, respectively. The h_j is the part of enthalpy that includes only changes in the enthalpy due to specific heat. S_h includes volumetric heat sources that you have defined and the heat generation rate from chemical reactions.

$$\frac{\partial}{\partial t}(\rho Y_i) + \nabla.(\rho \vec{v} Y_i) = -\nabla.\vec{J}_i + R_i + S_i \quad (5)$$

This choose to solve conservation equations for chemical species due to fluid composition of human raspatory and air surrounding are moist air and CO_2, Ansys Fluent predicts the local mass fraction of each species, Y_i , through the solution of a convection-diffusion equation for the i^{th} species that is mass fraction of vapour in humid gas.

$$\frac{\partial}{\partial t}(\rho k) + \frac{\partial}{\partial x_i}(\rho k u_i) = \frac{\partial}{\partial x_j}\left(\alpha_k \mu_{eff} \frac{\partial k}{\partial x_j}\right) + G_k + G_b + S_k \quad (6)$$

$$\frac{\partial}{\partial t}(\rho \varepsilon) + \frac{\partial}{\partial x_i}(\rho \varepsilon u_i) = \frac{\partial}{\partial x_j}\left(\alpha_\varepsilon \mu_{eff} \frac{\partial \varepsilon}{\partial x_j}\right) + C_{1\varepsilon}\frac{\varepsilon}{k}(G_k + C_{3\varepsilon}G_b) - C_{2\varepsilon}\rho\frac{\varepsilon^2}{k} - R_\varepsilon + S_\varepsilon \quad (7)$$

where ρ is fluid density, kis turbulence kinetic energy, εis the turbulence dissipation rate, u_i is velocity components, α_k and α_ε are inverse effective Prandtl numbers for k and ε, μ_{eff} is effective viscosity, $C_{1\varepsilon}, C_{2\varepsilon}$ and $C_{3\varepsilon}$ are turbulent model constants, these values, used by default in Ansys Fluent, are $C_{1\varepsilon}$=1.42 and $C_{2\varepsilon}$=1.68, R_ε is main difference between the RNG k-ε and standard k-ε models lies in the additional term in the ε equation, S_k and S_ε are user-defined source terms.

Modeling turbulent production in the *k-ε* models, the term G_k represents the generation of turbulence kinetic energy due to the mean velocity gradients, representing the production of turbulence kinetic energy, is modeled identically for RANS models. From the exact equation for the transport of *k*, this term is defined as:

$$G_k = -\rho\overline{u_i' u_j'}\frac{\partial u_j}{\partial x_i} \quad (8)$$

When a nonzero gravity field and temperature gradient are present simultaneously, G_b is the generation of turbulence kinetic energy due to buoyancy, this is given by:

$$G_b = \beta g_i \frac{\mu_t}{Pr_t}\frac{\partial T}{\partial x_i} \quad (9)$$

where Pr_t is the turbulent Prandtl number for energy, the default value is 0.85. The coefficient of thermal expansion, β, is defined as:

$$\beta = -\frac{1}{\rho}\left(\frac{\partial \rho}{\partial T}\right)_p \quad (10)$$

The constitutive relationship between air temperature, pressure and density is given by the ideal gas law (such model is sufficient because of small humidity of the gas involved in the considered multiphase flow):

$$p = \frac{\rho}{M}RT \quad (11)$$

where *R* is universal gas constant and *M* is molecular weight of the gas phase.

To track the trajectories and other valuable parameters of cough droplets and particles, a DPM model based on Lagrangian formulation is utilized. This force balance equates the particle inertia with the forces acting on the particle, and can be written as:

$$m_p\frac{d\vec{u}_p}{dt} = m_p\frac{\vec{u}-\vec{u}_p}{\tau_r} + m_p\frac{\vec{g}(\rho_p-\rho)}{\rho_p} + \sum \vec{F}_i \quad (12)$$

where m_p is the particle mass, $\vec{u}$is the fluid phase velocity, $\vec{u}_p$ is the particle velocity, ρ is the fluid density, ρ_p is the density of the particle, $\sum \vec{F}_i$ is an additional force *i* denotes particle *i*, $m_p(\vec{u}-\vec{u}_p)/\tau_r$ is the drag force, F_D, and τ_r is droplet or particle relaxation time calculated by:

$$\tau_r = \frac{\rho_p d_p^2}{18\mu}\frac{24}{C_d Re} \quad (13)$$

here, μ is the molecular viscosity of the fluid, $d_p$is the particle diameter, for smooth particles the drag coefficient, C_d, can be taken from

$$C_d = a_1 + \frac{a_2}{Re\frac{a_3}{Re^2}} \quad (14)$$

where a_1, a_2, and a_3 are constants that apply over several ranges of Reynolds number (Re) that is the relative, which is defined as:

$$Re \equiv \frac{\rho d_p|\vec{u}_p-\vec{u}|}{\mu}. \quad (15)$$

In Eq. 12 incorporates additional forces in the particle force balance that can be important under special circumstances. The first of these is the "virtual mass" force, the force required to accelerate the fluid surrounding the particle. C_{vm} is the virtual mass coefficient. This force can be written as:

$$\vec{F}_{\text{i,vir}} = C_{vm}m_p\frac{\rho}{\rho_p}\left(\vec{u}_p\nabla\vec{u} - \frac{d\vec{u}_p}{dt}\right) \quad (16)$$

Small particles suspended in a gas that has a temperature gradient experience a force in the direction opposite to that of the gradient. This phenomenon is known as thermophoresis force, $\vec{F}_T$. Ansys Fluent can optionally include a thermophoretic effect on particles in the additional force,

$$\vec{F}_T = -D_{T,p}\frac{1}{T}\nabla T \quad (17)$$

where $D_{T,p}$is the thermophoretic coefficient. You can define the coefficient to be constant, polynomial, or a user-defined function, or you can use the form suggested by Talbot:

$$D_{T,p} = \frac{6\pi d_p \mu^2 C_s(K+C_tKn)}{\rho(1+3C_mKn)(1+2K+2C_tKn)} \quad (18)$$

where Kn is Knudsen number $(2\lambda/d_p)$ that this expression assumes that the particle is a sphere, λ is mean free path of the fluid, $K = k/k_p$, *k* is fluid thermal conductivity based on translational energy only = $(15/4)\mu R$, *T* is local fluid temperature, μ is fluid viscosity, C_m = 1.14, C_s= 1.17, and C_t = 2.18.

The Saffman's lift force, $\vec{F}_{Saffman}$, or lift due to shear, can also be included in the additional force term as an option. The lift force used is a generalization of the expression provided by Saffman:

$$\vec{F}_{Saffman} = m_p\frac{2Kv^{1/2}\rho d_{ij}}{\rho_p d_p(d_{lk}d_{kl})^{1/4}}(\vec{u}-\vec{u}_p) \quad (19)$$

where *K* and $d_{ij}$is the deformation tensor. This form of the lift force is intended for small particle Reynolds numbers and is recommended only for sub-micron particles.

Brownian motion arises because of individual collisions between molecules and particles. These collisions will lead to

a sort of particle diffusion. Brownian motion is only important for sub-micron particles. Since only a small fraction of the cough droplet particles have a diameter in the order of 1 μm the Brownian motion was considered superfluous for the simulations. The modeling of Brownian motion resembles that of turbulent dispersion. Brownian motion is modeled as white noise. The force components are modeled with the product of a Gaussian distributed random number and the square root of the spectral intensity, $S_{n,ij}$ given by:

$$S_{n,ij} = S_0 \delta_{ij} \tag{20}$$

where δ_{ij} is the Kronecker delta function, and

$$S_0 = \frac{216 v k_B T}{\pi^2 \rho d_p^5 \left(\frac{\rho_p}{\rho}\right)^2 C_c} \tag{21}$$

where T is the absolute temperature of the fluid, v is the kinematic viscosity, C_c is the Cunningham correction, and k_B is the Boltzmann constant. Amplitudes of the Brownian force components are of the form

$$F_{b_i} = m_p \zeta_i \sqrt{\frac{\pi S_0}{\Delta t}} \tag{22}$$

where ζ_i are zero-mean, unit-variance-independent Gaussian random numbers. The amplitudes of the Brownian force components are evaluated at each time step. The energy equation must be enabled for the Brownian force to take effect. Brownian force is intended only for laminar simulations. The drag function is expressed as:

$$F_D(u - u_p) = \frac{\mu}{p_d d_p^2} \frac{18 C_D Re}{24(u - u_p)} \tag{23}$$

for sub-micron particles, a form of Stokes' drag law is available. In this case, is defined as:

$$F_D = \frac{18\mu}{d_p^2 \rho_p C_c}, \tag{24}$$

the factor is the Cunningham correction to Stokes' drag law, which you can compute from

$$C_c = 1 + \frac{2\lambda}{dp}\left(1.257 + 0.4 e^{-\left(1.1 d_p / 2\lambda\right)}\right) \tag{25}$$

where, λ is the molecular mean free path.

The dispersion of particles due to turbulence in the fluid phase, this work was predicted using the stochastic tracking model. Ansys Fluent uses a stochastic method (random walk model) to determine instantaneous gas velocity. In the Discrete Random Walk (DRW) model, the fluctuating velocity components are discrete piecewise constant functions of time. Their random value is kept constant over an interval of time given by the characteristic lifetime of the eddies. Discrete phase modeling can model the reacting particles or droplets and the effect on continuous phases can be examined. The relationship of heat and mass transfer, known as the "law", is contained in Ansys Fluent and the physical model used in multi-component particle definition (Law 7). The particle mass m is the sum of the masses of the components,

$$m = \sum_i m_i \tag{26}$$

The density of the particle can be either constant, or volume-averaged:

$$\rho_p = \left(\sum_i \frac{m_i}{m \rho_i}\right)^{-1} \tag{27}$$

The multicomponent droplet vaporization rate is calculated as the sum of the vaporization rates of the individual components. For the diffusion-controlled vaporization model, the vaporization rate of component is given by:

$$\frac{dm_i}{dt} = A_p M_w k_{c,i}\left(C_{i,s} - C_{i,\infty}\right) \tag{28}$$

when the rate of vaporization is slow, it can be assumed to be governed by gradient diffusion, with the flux of droplet vapor into the gas phase related to the difference in vapor concentration at the droplet surface and the bulk gas:

$$N_i = k_{c,i}\left(C_{i,s} - C_{i,\infty}\right) \tag{29}$$

where m_i is mass of component i in droplet (kg), $k_{c,i}$ is mass transfer coefficient of component i (m/s) and N_i is molar flux of vapor (kmol/m^2-s),$A_p$is droplet surface area (m^2),$C_{i,s}$and $C_{i,\infty}$are concentration of species at the droplet surface and the bulk, respectively (kmol/m^3).

The concentration of vapor at the droplet surface is evaluated by assuming that the partial pressure of vapor at the interface is equal to the saturated vapor pressure, p_{sat}, at the droplet temperature, T_p :

$$C_{i,s} = \frac{p_{sat}(T_p)}{R T_p} \tag{30}$$

where R is the universal gas constant.

The concentration of vapor in the bulk gas is known from solution of the transport equation for species i as:

$$C_{i,\infty} = X_i \frac{p}{R T_\infty} \tag{31}$$

where X_i is the local bulk mole fraction of species i, p is the local pressure, and T_∞ is the local bulk temperature in the gas. The mass transfer coefficient in Eq.29 is calculated from the Sherwood number correlation:

$$Sh_{AB} = \frac{k_c d_p}{D_{i,m}} = 2.0 + 0.6\, Re_d^{1/2}\, S\, c^{1/3} \tag{32}$$

where $D_{i,m}$ is diffusion coefficient of vapor in the bulk (m^2/s),$Sc$is the Schmidt number $\left(\mu/\rho D_{i,m}\right)$,and$d_p$is particle (droplet) diameter (m). While for the convection/diffusion-controlled model, it is given by:

$$\frac{dm_i}{dt} = A_p k_{c,i} \rho\, ln\left(1 + B_{m,i}\right) \tag{33}$$

whereρ is gas density (kg/m^3), M_w is molecular weight of species, i, and $B_{m,i}$is the Spalding mass number.

$$B_m = \frac{Y_{i,s} - Y_{i,\infty}}{1 - Y_{i,s}} \tag{34}$$

where $Y_{i,s}$ is vapor mass fraction at the surface, $Y_{i,\infty}$is vapor mass fraction in the bulk gas. The energy equation is written for the multicomponent particle as follows:

$$m_p c_p \frac{dT}{dt} = h A_p\left(T_\infty - T_p\right) + \sum_i \frac{dm_i}{dt}\left(h_{vap,i}\right) \tag{35}$$

where dm_i/dt is computed from Eq.28 and 33, $h_{vap,i}$is latent heat of vaporization for component i, h is heat transfer coefficient for the diffusion-controlled vaporization model as follows:

$$Nu = \frac{h d_p}{k_\infty} = 2.0 + 0.6\, Re_d^{1/2}\, Pr^{1/3}, \tag{36}$$

where Nu is the Nusselt number, $k_\infty$is thermal conductivity of the continuous phase (W/m-K), Re_d is Reynolds number based on the particle diameter and the relative velocity. The exchange of mass and energy between liquid droplets of cough or sneeze and the surrounding gases was calculated droplet by

droplet. After the temperature of each droplet is calculated, the amount of vaporized liquid is added to the mesh cell and the gas temperature in the cell is balanced according to the energy exchange between the droplet and the surroundings.

To simulate evaporation of water into so-called solid particles, multi-component particles are used in conjunction with a user-defined function (UDF). Multi-component particles can inject particles containing more than one substance, such as saliva and viruses. However, with the Ansys Fluent program, only liquid particles can be represented as multi-components. Hence, it is necessary to create a multi-component particle consisting of water and additional liquids later to further change the liquid properties and to later represent real solids. In this simulation, the cough droplets were assumed by using droplets of two mass fraction evaporating species as 98.2% water and 1.8 % urea water as density of 1,000 kg/m^3, the water was determined to be vaporizing and the urea water not-vaporizing. From heat and mass transfer relationships, the evaporation of the species in the droplets can be seen and the reduction of droplet diameter until the final size can be observed.

3. Introduction Geometry, mesh generation, and boundary conditions

The droplet evaporation and dispersion were studied by using numerical simulations to understand the basic aerosol science of SARS-CoV-2-laden droplets spread through the air in an indoor environment. This methodology begins with a review of the relevant literature to search for numerical models that can predict the behavior of droplet evaporation to droplet nuclei so-called solid aerosol. Due to the limitation of the HPC license on Ansys Fluent, the computational domain of cuboid space in front of a coughing person's mouth was assumed using the 2D model with the geometry of 4 m-length and 3 m-height, as shown in Fig. 1. The geometry model was divided into two zones, so-called near mount zone and the rest zone to assign different grid sizing. The geometry domain was discretized using structured hexahedral grids with very fine mesh applied at the near mount zone and rest zone defined as coarse mesh.

The center of the mouth is strictly placed at 2.0 m in vertical distance of the left-hand side of the domain. The inlet boundary condition has a hydraulic diameter of 0.02 m, which represents the human mouth opening for coughing as assigned the velocity, the temperature, and humidity with same environment air. The coughing velocity can be assigned as velocity constant of cough jet and pulse of single cough. The right-hand side of the domain was set as a pressure outlet with zero-gauge pressure, which considered the ambient conditions as the air temperature and humidity. The non-slip boundary conditions have been used for all other walls where isothermal condition was assumed. The data in boundary conditions of each computational case are listed in Table 1.

Generally, the human cough is a variable flow rate. However, by integrating the flow rate profile along the time axis we obtain an average velocity value of 10 m/s.[29,30]

Table 1. Boundary conditions of the parametric study cases.

Case No.	Inlet: Velocity inlet U_0 = 10 [m/s]			Ambient conditions		Outlet: Pressure outlet		Wall: Adiabatic wall
	T_{in} (°C)	RH (%)	U_0 [m/s]	T_∞ (°C)	RH (%)	T_∞ (°C)	RH (%)	DPM
1	25	0	10	25	0	25	0	Trap
2	25	0	Pulse	25	0	25	0	Trap
3	25	60	10	25	90	25	90	Trap
4	15	60	10	15	60	18	60	Trap
5	25	60	10	25	60	25	60	Trap
6	35	60	10	35	60	35	60	Trap
7	45	60	10	45	60	45	60	Trap

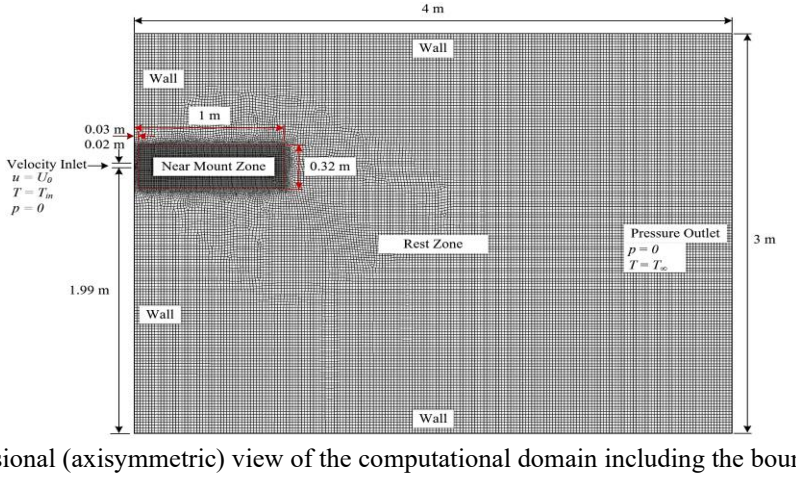

Fig. 1 Schematic two-dimensional (axisymmetric) view of the computational domain including the boundary conditions for the case of caught droplet in static ambient air condition and computational grid.

Therefore, the variable flow rate of the coughing jet at an average velocity of 10 m/s was prescribed for the air leaving the mouth in the inlet boundary condition. For pulse of a single cough was prescribed by the velocity at 10 m/s within 0.5 s.

The first step was model geometry and grid, we used the design modeler and mesh using the Ansys Workbench program. For physical setup and simulations, the governing equations were discretized based on a finite-volume method and solved using the commercial CFD code of Ansys Fluent software. The multi-component Eulerian-Lagrangian model was applied to realize the droplet evaporation process, in which the RNG k-ε model was coupled with the DPM model, energy equation, and species transport equation. The DPM model is adopted to calculate the evaporation and transmission process of droplets in the continuous air background, which is reasonable as the expelled saliva/phlegm droplets are assumed to be composed of 98.2% water and 1.8% as urea-water with the same density as not-vaporizing. The heat and mass exchanges exist between the liquid droplet surface and the ambient air. The time step was 0.01 s for all simulation periods. The three different meshes called Mesh 1, Mesh 2, and Mesh 3 were generated to find out the least required amount of meshes. The mesh sizes are divided into 3 parts. The mesh size of inlet BC is 5 mm. The mesh size of the near mount zone and rest zone are particularly adjusted by 5 to 20 mm, which mesh is generated as 33,199, 43,255, and 131,136 elements, respectively (see Table 2). The velocity inlet BC of case 1 is cough jet and case 2 is the pulse of a single cough in which the temperature of dry air (RH = 0%) and droplet is 25 °C. The droplet evaporation with an initial diameter of 10, 50, and 100 µm are calculated to reach their equilibrium diameters using the simulation periods of 10 s. The DPM injections are prescribed by the surface released at inlet BC, in which the droplets are injected by 4 particles per time step and every 0.01 s until 10 s for cough jet to always report a diameter reduction with the current position of particle tracks and for until to 0.5 s of for pulse of a single cough. For the pulse of a single cough, the droplets are injected by 4 particles per time step and every 0.01 s until 0.5 s.

Table 2. Three meshes used in the grid independence test.

Mesh No.	Element size at inlet (mm)	Element size at near mount zone (mm)	Element size at rest zone (mm)	Total elements
Mesh 1	5	10	20	33,199
Mesh 2	5	5	20	43,255
Mesh 3	5	5	10	131,136

Case 3 is the validation process, in which the predicted time-dependent droplet diameter (solid lines) is compared against the reference work.[23] The boundary conditions are set as the evaporation of droplets falling freely in quiescent air, according to the literature paper, which two single droplets sizes (10 and 100 µm) and very small droplet mass flow rates (5.24×10^{-11} kg/s for the 10-µm droplets and 5.24×10^{-8} kg/s for the 100-µm droplets, respectively) are used to match the computational conditions of the reference work. The velocity inlet BC is cough jet, which assumed the droplets are released with a time interval of 0.01 s until 100 s. The computations are conducted with a constant temperature of air and droplets of 25 °C. The relative humidity fields were changed from 0% became 90% respectively.

In cases 4 to 7, the relative humidity 30%–60% is quite suitable for most residents, but virus survival in droplets is determined at 60% relative humidity. Therefore, the size reduction until became droplet nuclei and trajectory of the cough droplets were predicted to study the influent temperatures with specific relative humidity at 60% RH. The assumptions of air temperature and relative humidity of the inlet and environment are the same because the exhaled air is more dilute. The different temperature is 15, 25, 35, and 45 °C that species mass fraction of water vapor and air density follow in Table 3. The different initial droplet diameter, *i.e.*, 10, 20, 30, 40, 50, 60, 70, 80, 90, 100, 120, 140, 150, 160, 175, 200, 225, 250, 275, and 300 µm, are injected with the same velocity of 10 m/s, and the injection frequency is 0.01 s for the simulation periods of 35 s. The droplets will be trapped when they contact the wall or fall onto the ground.

Table 3. The air properties of mass fraction of species and densities.

T (°C)	RH (%)	Species Mass Fraction	Density (kg/m^3)
15	60	0.00631	1.207
25	60	0.01175	1.175
35	60	0.02099	1.131
45	60	0.03610	1.086

4. Results and discussion

4.1 Mesh independent

The simulation results of Case 1 and Case 2, three different meshes (see Table 2) were generated and the evaporation in dry air of droplets with initial diameters of 10, 50, and 100 µm were calculated to find out the least required amount of meshes. The mesh independent was achieved at the number of droplet trajectories was also analyzed. It found that when the mesh number was larger than 33,199. Fig. 2 shows that the results of the three meshes almost overlap with each other. Moreover, Fig. 3 shows droplet suspension patterns at different time stations of Case 2 of varying droplet sizes in dry air. Some small differences exist probably due to the occasionality of numerical simulation. Thus, the grid independence of meshes has been verified and the smallest mesh (Mesh 2) is used in the following simulations.

4.2 Validation results

The predicted time drop diameter (solid line) was compared with the theoretical calculation (marker) by Li *et al.*,[22] as

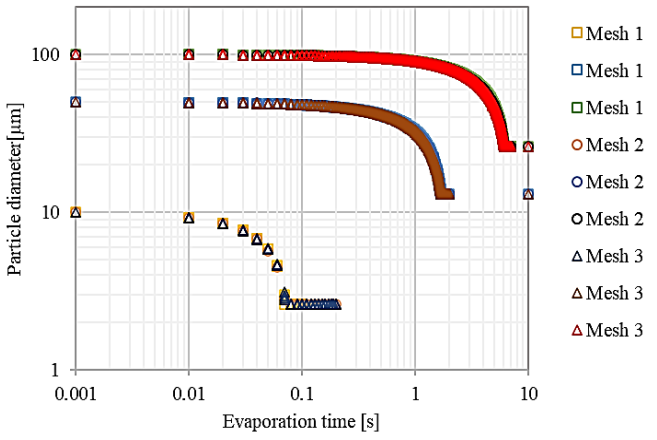

Fig. 2 Effect of grid independent on the droplet diameter shrinks over time of varying droplet sizes as 10, 50 and 100 μm in dry air (T_p =25 °C, T_∞ = 25 °C, RH = 0%, U_0 = 10 m/s).

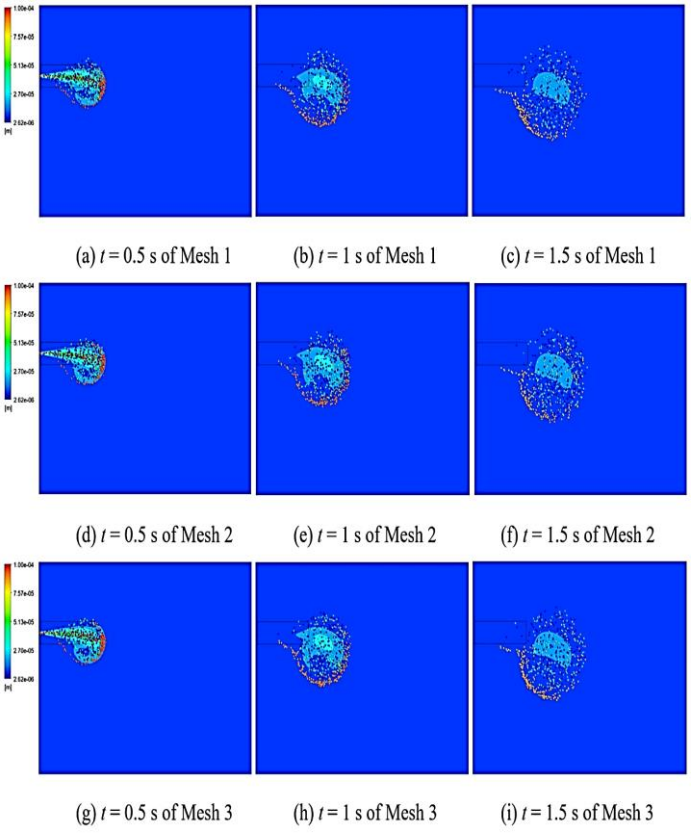

Fig. 3 Effect of mesh independent on droplet suspension patterns at different time stations of Case 2 of varying droplet sizes as 10, 50 and 100 μm in dry air (T_p =25 °C, T_∞ = 25 °C, RH = 0%, and U_0 = 10 m/s).

shown in Fig. 4. There was a satisfactory tendency between the numerical results of this study and the validation data that the literature referenced for both the initial droplet size and the relative humidity of the air. The figure also reveals that droplet evaporation is sensitive to both parameters (initial size and relative humidity). First, the evaporation rate is greatly affected by droplet size. Smaller droplets evaporate faster than larger droplets over a considerable time difference due to the enlarged specific surface area for heat and mass transfer. Second, the relative humidity of the air plays an important role. The relative humidity was changed from 0% to 90%, the evaporation time to equilibrium diameter of droplets nuclei increases dramatically from 0.075 s to 0.55 s for 10 μm droplets and from 6.03 seconds to 33.4 seconds.

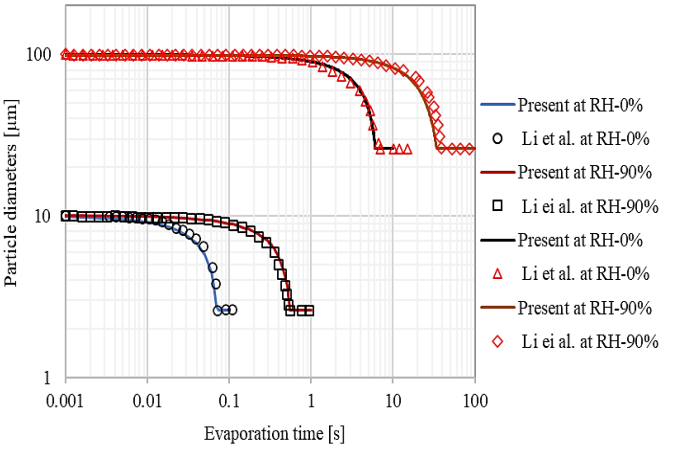

Fig. 4 Model validation using data of Li *et al.* [23] both 0% relative humidity and 90% relative humidity (T_p =25 °C, T_∞ = 25 °C, U_0 = 10 m/s).

4.3 The effects of the different room temperatures

Due to some results are close together and similar. Therefor the evaporation-induced size reduction results of different droplet size, *i.e.*, 10, 20, 30, 40, 60, 100, 120, 140, 150, 160, 175, 200, 225, 250, 275, and 300 μm, with time-dependent are shown in Fig. 5, the line colors shows the effect of different room temperature levels (blue line of 15 °C, green line of 25 °C, black line of 35°C and red line of 45 °C). In the numerical setting, we set the initial temperature of the cough droplets at 33˚C, and the ambient temperature at 15, 25, 35, and 45 °C, respectively with same RH. The droplet sizes as different initial sizes were injected into the computational domain using different boundary conditions in the cases 3 to 6, respectively. The droplets are evaporated completely as long as the trajectory float in the domain, and evaporation is canceled when the droplets were trapped and escape the domain boundaries. It is found the evaporation of droplet sizes of about 10-120 μm was found that the droplets were evaporated completely until they became solid aerosols in a short time. The higher temperatures have the effect of fast evaporating until final sizes as solid aerosols about 26.2% of initial particle diameters. The evaporation of 140-300 μm droplets is canceled within 5 seconds of evaporation time due to the droplets falling to the wall boundary. The lowest temperature at 15 °C was slightly longer evaporation time than higher temperatures, which the other cases have a close evaporation time.

The completed evaporation time of different droplet size for 10-120 μm and the end of evaporation time for the bigger size were collected to plot the relation curves of evaporation time vs. initial particle diameter, and vs. final particle diameter as shown in Fig. 6. In the same figure, primary plot of curves

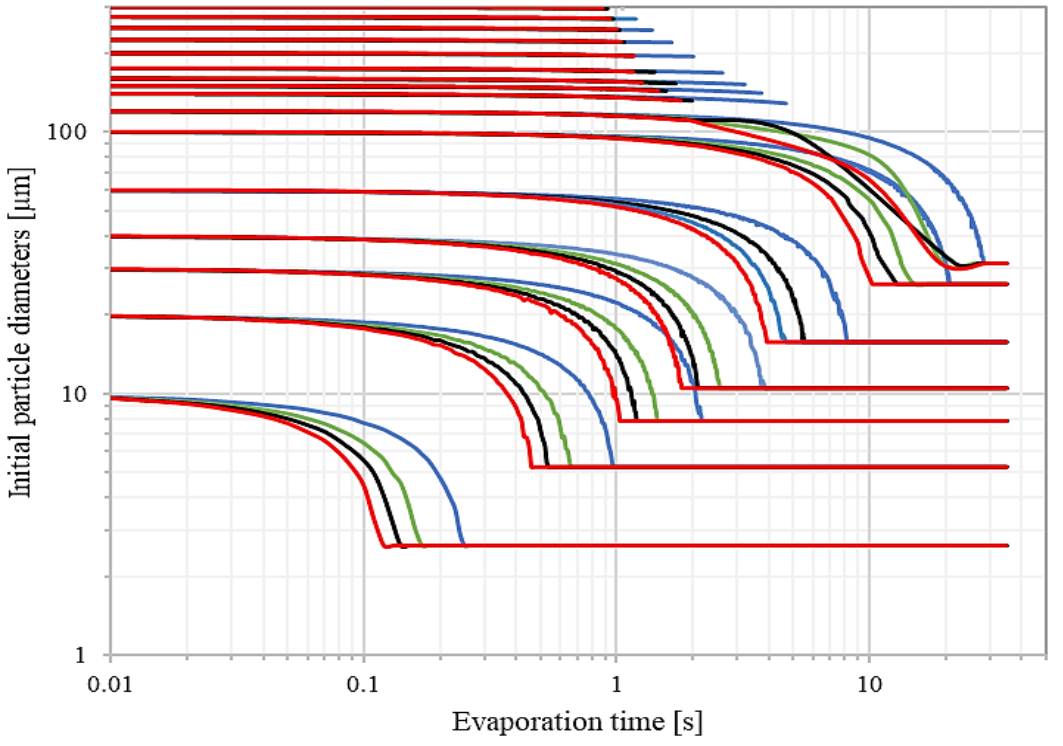

Fig. 5 The size reduction versus evaporation time of the droplets of different initial sizes, *i.e.*, 10, 20, 30, 40, 60, 100, 140, 150, 160, 175, 200, 225, 250, 275, and 300 µm of different ambient temperature (— blue line of 15 °C, — green line of 25 °C, — black line of 35 °C and — red line of 45 °C).

is initial particle diameters (x-axis) versus evaporation time (y-axis) as different ambient temperatures that result found the higher the temperature has the effect to decrease completed evaporation time for initial particle diameters of 10-120 µm. The evaporation time was canceled in the short time for initial particle diameters 140-300 µm, but the evaporation not completed due to the droplet particles dropped on the bottom wall boundary, which evaporation time can be called falling time. The secondary diagram is curves of final particle diameter vs. evaporation time. In the results revealed that the initial particle diameter of 10-120 µm was completely evaporated within 5s and the initial particle diameter 140-300 µm was not completely evaporation, which the final size has been reduced only slightly due to the droplets falling to the wall boundary.

Figure 7 show the x-y trajectories vs falling time of six different diameters droplets such as 100, 120,150, 200, 250, and 300 µm at different ambient temperatures., *i.e.*, 15, 25, 35, and 45 °C within 35 s. The y-axis of the primary plot is the vertical distance of domain height (orange line of 15 ˚C, gold line of 25 ˚C, green line of 35 °C and dark orange line of 45 °C). And the y-axis of the secondary plot is the horizontal distance of domain width (red line of 15 °C, black line of 25 °C, blue line of 35˚C and dark blue line of 45 °C), which the horizontal distance can be provided to evaluate the social distancing.

Figures 7a and 7b show the x-y trajectories with time-dependent of 100 and 120 µm, it was found that droplet motion was quite difficult to determine trajectory both vertically and horizontally at any time. However, droplets were floating and dissipation in the all-around the domain, which the droplet size ≤ 120 µm could be successfully evaporated to be solid aerosols. The x-y trajectories as Fig. 7c, the falling time of droplet size 150 µm at temperatures 15, 25, 35, and 45 °C were 3.74, 1.49, 1.57, and 1.46 s, respectively, and 0.727, 3.21, 3.82, and 3.34 m, respectively for horizontal distance. The x-y trajectories as Fig. 7d, the falling time of droplet size 200 µm at temperatures 15, 25, 35, and 45 ˚C were 2.01, 1.02, 1.16, and 1.17 s, respectively, and 1.39, 3.01, 3.01, and 3.05 m, respectively for horizontal distance. The x-y trajectories as Fig. 7e, the falling time of droplet size 250 µm at temperatures 15, 25, 35, and 45 °C were 1.38, 0.98, 1.03, and 1 s, respectively, and 2.15, 3.24, 3.24, and 3.23 m, respectively for horizontal distance. Finally, the x-y trajectories as Fig. 7f, the falling time of droplet size 300 µm at temperatures 15, 25, 35, and 45 °C were 1.06, 0.91, 0.92, and 0.88 s, respectively, and 2.98, 3.69, 3.75, and 3.82 m, respectively for horizontal distance. In above results found that the lowest temperature at 15 °C has a slightly longer evaporation time than higher temperatures, while the other cases have a close evaporation time. This temperature has significantly the shortest falling time and the shortest horizontal distance, in which the other cases both falling time and horizontal distance were approximately the same.

Figures 8 to 11 show the cough droplet jet with 10 m/s from the human mouth that compare the droplet distributions of different initial diameter (every 10 µm between 10 µm and 160 µm, every 25 µm between 247 µm and 300 µm) of predicted results with different temperature (15, 25, 35, and 45 °C) and same RH at 0.5 s, 1 s to 5 s in quasi-quiescent air. It can be

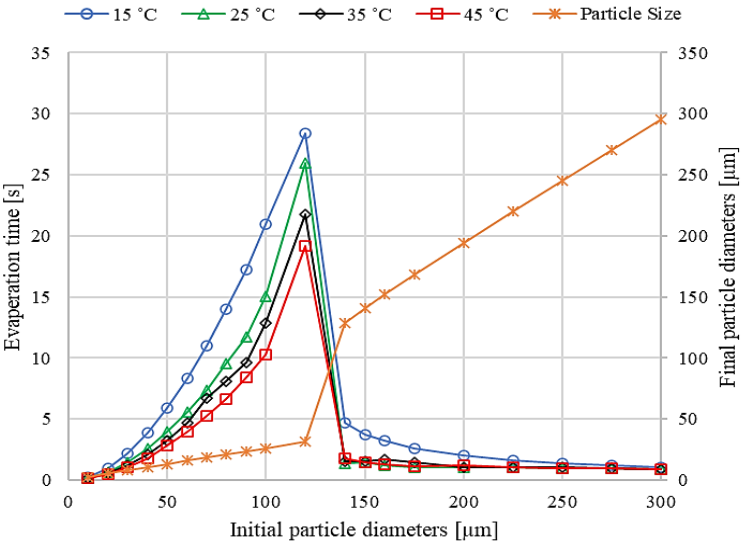

Fig. 6 The evaporation time vs initial particle diameters vs final particle diameters curves of droplets at different temperatures levels.

seen that, the cough droplet jet can freely develop, and the droplets travel along with the jet flow under quasi-quiescent air in an indoor environment. The higher temperatures have to influent faster dropping and farther horizontal distances, but the lower temperature tends to more vertical distance.

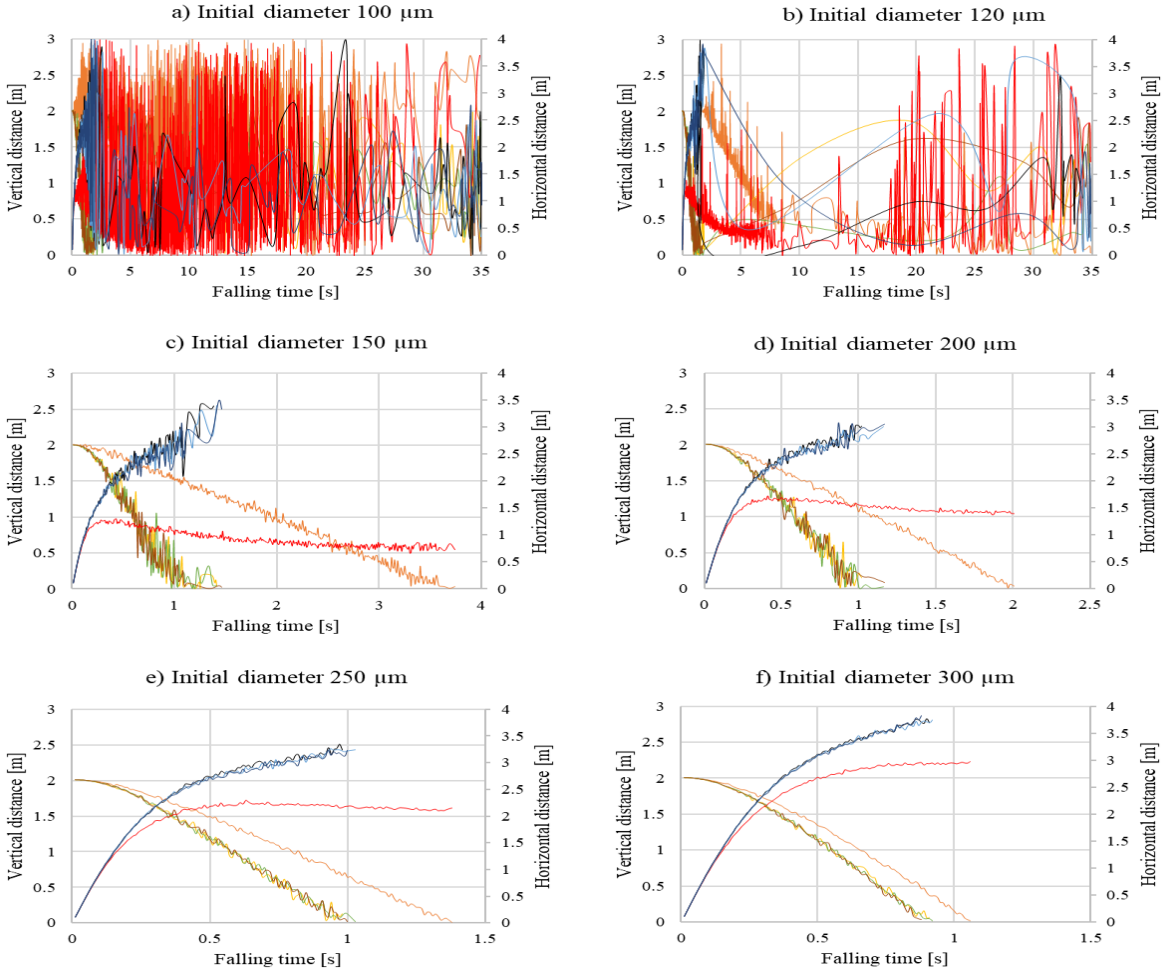

Fig. 7 The x-y trajectories of droplets of six different diameters at different ambient temperature, *i.e.*, 15, 25, 35, and 45 °C, different diameter seem in the chart title.

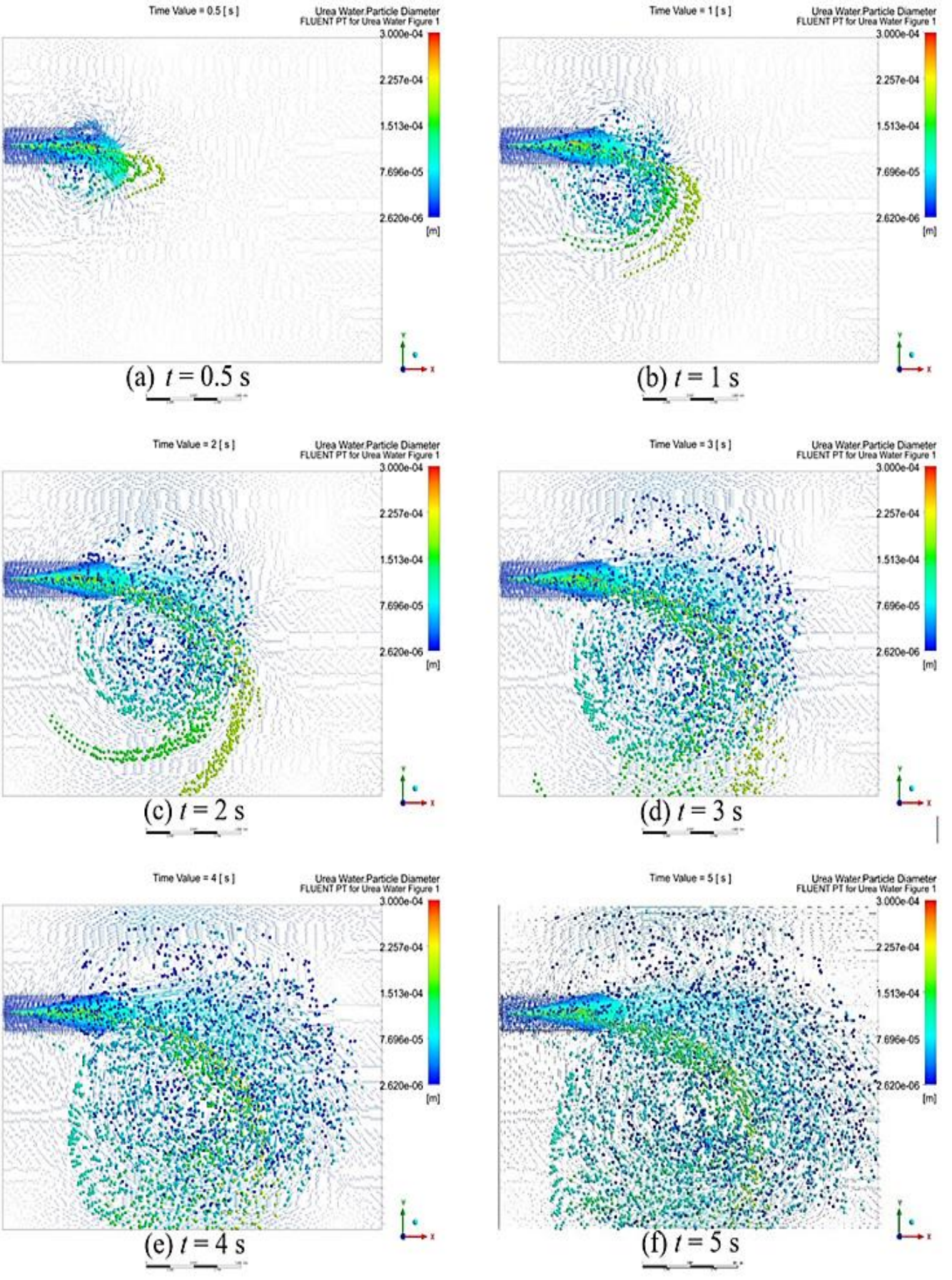

Fig. 8 Comparison the droplet size distributions of cough jet results with 15 °C and 60% RH in quasi-quiescent air at: (a) t = 0.5 s, (b) t = 1 s, (c) t = 2 s, (d) t = 3 s, (e) t = 4 s, (f) t = 5 s.

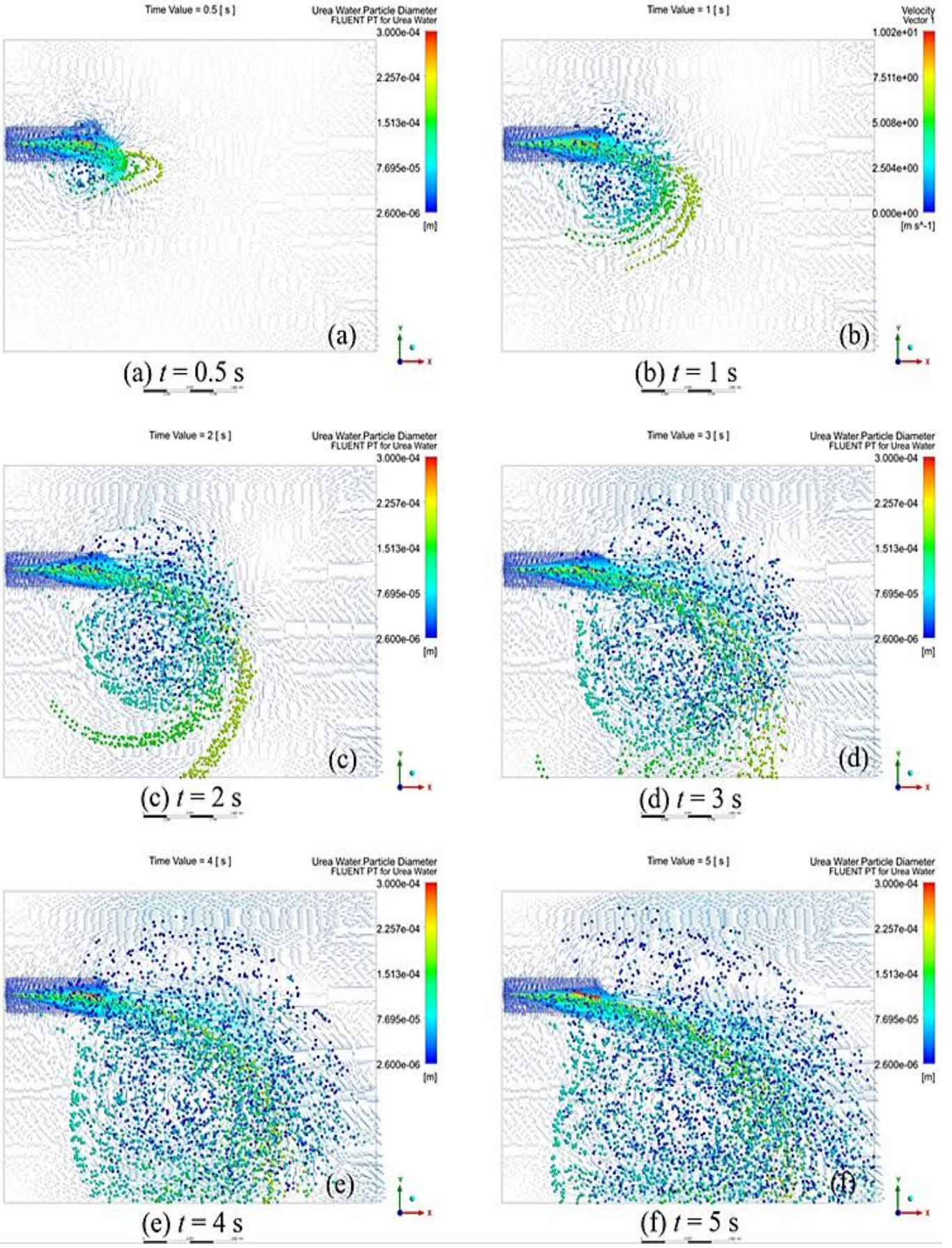

Fig. 9 Comparison the droplet size distributions of cough jet results with 25 °C and 60% RH in quasi-quiescent air at: (a) t = 0.5 s, (b) t = 1 s, (c) t = 2 s, (d) t = 3 s, (e) t = 4 s, (f) t = 5 s.

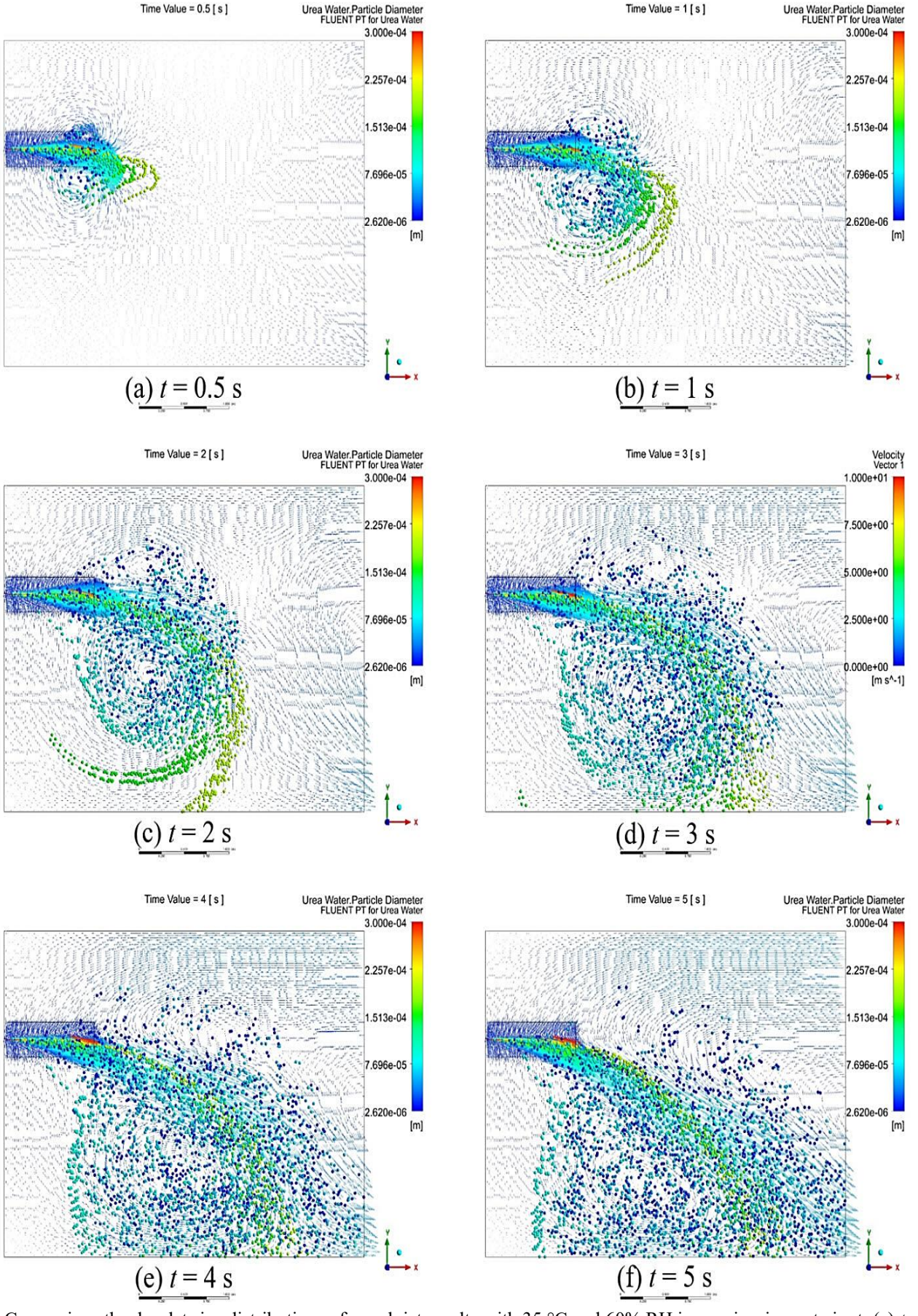

Fig. 10 Comparison the droplet size distributions of cough jet results with 35 °C and 60% RH in quasi-quiescent air at: (a) t = 0.5 s, (b) t = 1 s, (c) t = 2 s, (d) t = 3 s, (e) t = 4 s, (f) t = 5 s.

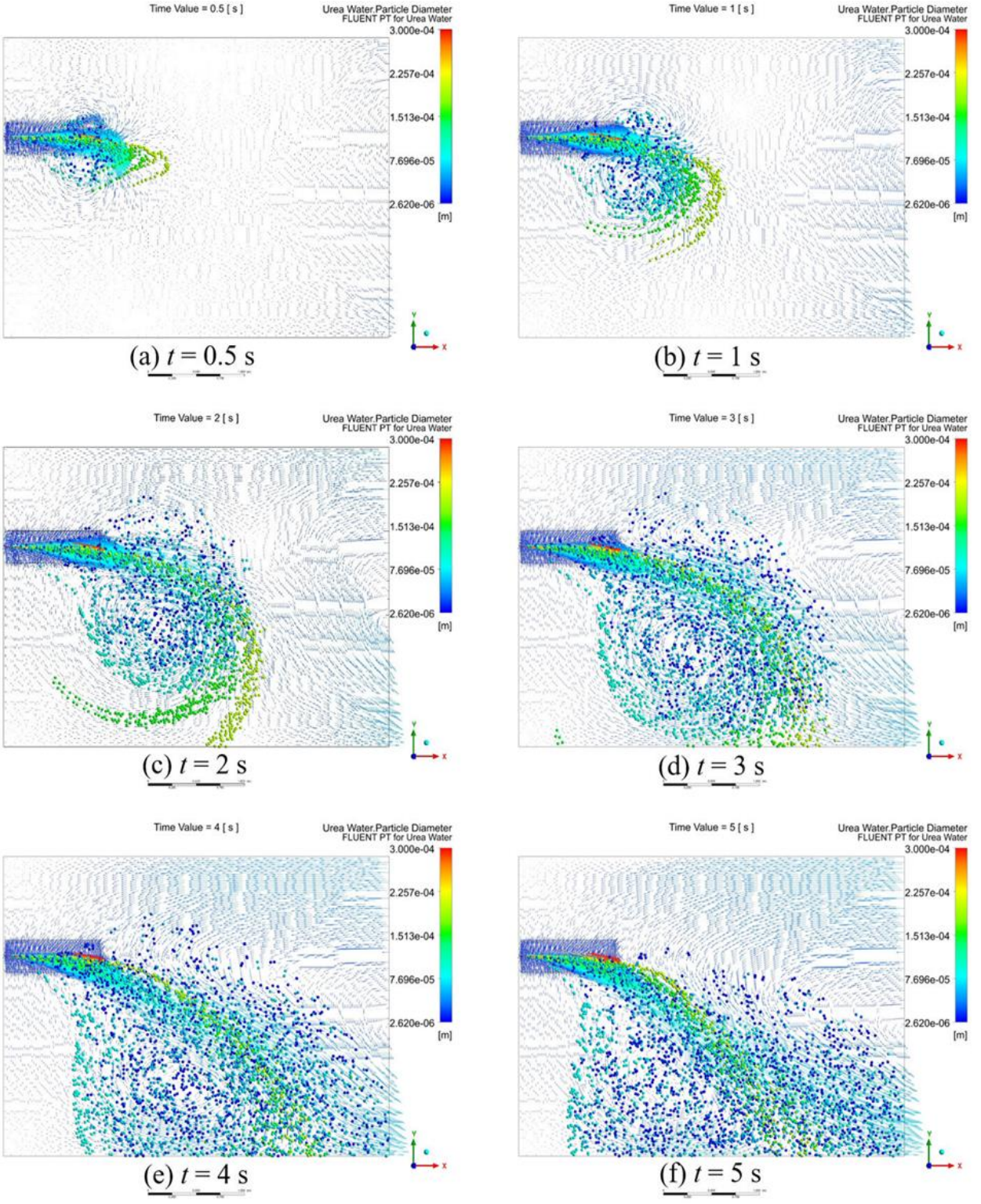

Fig. 11 Comparison the droplet size distributions of cough jet results with 45 °C and 60% RH in quasi-quiescent air at: (a) t = 0.5s, (b) t = 1 s, (c) t = 2 s, (d) t = 3 s, (e) t = 4 s, (f) t = 5 s.

5. Conclusion

The numerical simulation investigated cough droplet evaporation and diffusion in quiescent air and was verified by comparing the current simulation data with the data in literature. The cough droplets at 10 and 100 μm evaporate at 25 °C with air relative humidity of 0 and 90%. The evaporation time, falling time, and direction of difference diameters (*i.e.*, 10, 20, 30, 40, 60, 100, 120, 140, 150, 160, 175, 200, 225, 250, 275, and 300 μm) of cough droplets at 15, 25, 35, and 45 °C and 60% RH are determined by the room temps. The following are the findings of this investigation:

a) The validation results of this study were consistent with the

reference data, for both initial droplet diameter at 10 μm and 100 μm and air relative humidity of 0 and 90%.
b) The evaporation rate is greatly affected by droplet size, which the smaller droplet evaporates faster than larger droplet over a considerable time difference due to the enlarged specific surface area for heat and mass transfer.
c) The higher relative humidity of the air plays an important role to increase evaporation time.
d) The higher temperatures of the environment can accelerate the mass transfer to be fast evaporating than lower temperatures.
e) The evaporation of initial droplet diameter ≤ 120 μm was completely evaporated until became droplet nuclei in a short time about 26.2% of initial diameters because the droplets were floating and dispersing still within the domain.
f) The evaporation time or falling time of initial droplet diameter ≥ 140 μm was canceled within 5 seconds due to the droplets falling to trap the bottom wall boundary.
g) The lowest temperature at 15 °C has a slightly longer evaporation time than higher temperatures, while the other cases have a close evaporation time. This temperature has significantly the shortest falling time and the shortest horizontal distance because the residual droplet mass was greater than in the other cases, in which the other cases both falling time and horizontal distance were approximately the same.

Finally, still, there are some limitations in this work. For instance, the droplet evaporation is canceled when the droplets drop to walls because the wall film model in the DPM model is not used in the wall boundary condition. The transient processes of coughing and the three-dimension model can be worth future study.

Acknowledgements
This study was supported by the National Research Council of Thailand (Grant Number N42A650197), Thailand Science Research and Innovation Fundamental Fund (TUFF41/2566) and Thammasat University Research Fund.

Conflict of Interest
There is no conflict of interest.

Supporting Information
Applicable.

References
[1] Y. Feng, T. Marchal, T. Sperry, H. Yi, Influence of wind and relative humidity on the social distancing effectiveness to prevent COVID-19 airborne transmission: a numerical study, *Journal of Aerosol Science*, 2020, **147**, 105585, doi: 10.1016/j.jaerosci.2020.105585.
[2] L. Bourouiba, A sneeze, *New England Journal of Medicine*, 2016, **375**, e15, doi: 10.1056/nejmicm1501197.
[3] L. Bourouiba, Fluid dynamics of respiratory infectious diseases, *Annual Review of Biomedical Engineering*, 2021, **23**, 547-577, doi: 10.1146/annurev-bioeng-111820-025044.
[4] L. Yang, X. Li, Y. Yan, J. Tu, Effects of cough-jet on airflow and contaminant transport in an airliner cabin section, *The Journal of Computational Multiphase Flows*, 2018, **10**, 72-82, doi: 10.1177/1757482x17746920.
[5] J. P. Duguid, The size and the duration of air-carriage of respiratory droplets and droplet-nuclei, *Epidemiology and Infection*, 1946, **44**, 471-479, doi: 10.1017/s0022172400019288.
[6] D. B. Kwak, H. D. Fischer, D. Y. H. Pui, Saliva droplet evaporation experiment and simple correlation of evaporation-falling curve under different temperatures and RH, *Aerosol and Air Quality Research*, 2023, **23**, 220409, doi: 10.4209/aaqr.220409.
[7] S. Peng, Q. Chen, E. Liu, The role of computational fluid dynamics tools on investigation of pathogen transmission: prevention and control, Science of the Total Environment, 2020, **746**, 142090, doi: 10.1016/j.scitotenv.2020.142090.
[8] W. F. Wells, On air-borne infection, *American Journal of Epidemiology*, 1934, **20**, 611-618, doi: 10.1093/oxfordjournals.aje.a118097.
[9] X. Xie, Y. Li, A. T. Y. Chwang, P. L. Ho, and W. H. Seto, How far droplets can move in indoor environments – revisiting the Wells evaporation–falling curve, *Indoor Air*, 2007, **17**, 211–225, doi:10.1111/j.1600-0668.2007.00469.x.
[10] Y. Ji, H. Qian, J. Ye, X. Zheng, The impact of ambient humidity on the evaporation and dispersion of exhaled breathing droplets: a numerical investigation, *Journal of Aerosol Science*, 2018, **115**, 164-172, doi: 10.1016/j.jaerosci.2017.10.009.
[11] T. Dbouk, D. Drikakis, On coughing and airborne droplet transmission to humans, *Physics of Fluids*, 2020, **32**, 053310, doi: 10.1063/5.0011960.
[12] T. Dbouk, D. Drikakis, On airborne virus transmission in elevators and confined spaces, *Physics of Fluids*, 2021, **33**, 011905, doi: 10.1063/5.0038180.
[13] D. Mirikar, S. Palanivel, V. Arumuru, Droplet fate, efficacy of face mask, and transmission of virus-laden droplets inside a conference room, *Physics of Fluids*, 2021, **33**, 065108, doi: 10.1063/5.0054110.
[14] H. Motamedi Zoka, M. Moshfeghi, H. Bordbar, P. A. Mirzaei, Y. Sheikhnejad, A CFD approach for risk assessment based on airborne pathogen transmission, Atmosphere, 2021, **12**, 986, doi: 10.3390/atmos12080986.
[15] F. Pourfattah, L.-P. Wang, W. Deng, Y.-F. Ma, L. Hu, B. Yang, Challenges in simulating and modeling the airborne virus transmission: a state-of-the-art review, *Physics of Fluids*, 2021, **33**, 101302, doi: 10.1063/5.0061469.
[16] J. Wang, M. Alipour, G. Soligo, A. Roccon, M. De Paoli, F. Picano, A. Soldati, Short-range exposure to airborne virus transmission and current guidelines, *Proceedings of the National Academy of Sciences*, 2021, **118**, e2105279118.
[17] L. Wu, X. Liu, F. Yao, Y. Chen, Numerical study of virus transmission through droplets from sneezing in a cafeteria, *Physics of Fluids*, 2021, **33**, 023311, doi: 10.1063/5.0040803.
[18] F. Wang, I. Permana, C. Chaerasari, K. Lee, T. Chang, D.

Rakshit, Ventilation performance evaluation of a negative-pressurized isolation room for emergency departments, *Healthcare*, 2020, **10**, 193, doi: 10.3390/healthcare10020193.
[19] B. N. Safa, M. R. Bahrani Fard, C. R. Ethier, Correction to: 'In vivo biomechanical assessment of iridial deformations and muscle contractions in human eyes' 2022 by Safa et al., *Journal of the Royal Society Interface*, 2022, **19**, 20210819, doi: 10.1098/rsif.2022.0108.
[20] C. Chen, B. Zhao, Some questions on dispersion of human exhaled droplets in ventilation room: answers from numerical investigation, *Indoor Air*, 2010, **20**, 95-111, doi: 10.1111/j.1600-0668.2009.00626.x.
[21] C. Yang, X. Yang, B. Zhao, Person to person droplets transmission characteristics in unidirectional ventilated protective isolation room: the impact of initial droplet size, *Building Simulation*, 2016, **9**, 597-606, doi: 10.1007/s12273-016-0290-7.
[22] X. Li, Y. Shang, Y. Yan, L. Yang, J. Tu, Modelling of evaporation of cough droplets in inhomogeneous humidity fields using the multi-component Eulerian-Lagrangian approach, *Building and Environment*, 2018, **128**, 68-76, doi: 10.1016/j.buildenv.2017.11.025.
[23] Y. Yan, X. Li, J. Tu, Thermal effect of human body on cough droplets evaporation and dispersion in an enclosed space, *Building and Environment*, 2019, **148**, 96-106, doi: 10.1016/j.buildenv.2018.10.039.
[24] H. Calmet, K. Inthavong, A. Both, A. Surapaneni, D. Mira, B. Egukitza, G. Houzeaux, Large eddy simulation of cough jet dynamics, droplet transport, and inhalability over a ten minute exposure, *Physics of Fluids*, 2021, **33**, 125122, doi: 10.1063/5.0072148.
[25] C. Yang, X. Zhang, X. Cao, J. Liu, F. He, Numerical simulations of the instantaneous flow fields in a generic aircraft cabin with various categories turbulence models, *Procedia Engineering*, 2015, **121**, 1827-1835, doi: 10.1016/j.proeng.2015.09.163.
[26] F. Wang, C. Chaerasari, D. Rakshit, I. Permana, Kusnandar, Performance improvement of a negative-pressurized isolation room for infection control, Healthcare, 2021, **9**, 1081, doi: 10.3390/healthcare9081081.
[27] H. Kotb, E. E. Khalil, Sneeze and cough pathogens migration inside aircraft cabins, *Energy*, 2020, **2**, 36-45.
[28] ANSYS, Inc., Ansys fluent theory guide, 2022.
[29] J. Wei, Y. Li, Enhanced spread of expiratory droplets by turbulence in a cough jet, *Building and Environment*, 2015, **93**, 86-96, doi: 10.1016/j.buildenv.2015.06.018.